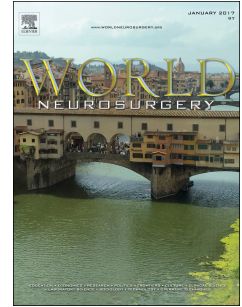


Accepted Manuscript

Impact of gradient number and voxel size on DTI tractography for resective brain surgery

Friso W.A. Hoefnagels, M.D., Philip C. de Witt Hamer, M.D., Ph.D., Petra J.W. Pouwels, Ph.D., Frederik Barkhof, M.D., Ph.D., W. Peter Vandertop, M.D., Ph.D.



PII: S1878-8750(17)30942-7

DOI: [10.1016/j.wneu.2017.06.050](https://doi.org/10.1016/j.wneu.2017.06.050)

Reference: WNEU 5921

To appear in: *World Neurosurgery*

Received Date: 27 November 2016

Revised Date: 5 June 2017

Accepted Date: 7 June 2017

Please cite this article as: Hoefnagels FWA, de Witt Hamer PC, Pouwels PJW, Barkhof F, Vandertop WP, Impact of gradient number and voxel size on DTI tractography for resective brain surgery, *World Neurosurgery* (2017), doi: 10.1016/j.wneu.2017.06.050.

This is a PDF file of an unedited manuscript that has been accepted for publication. As a service to our customers we are providing this early version of the manuscript. The manuscript will undergo copyediting, typesetting, and review of the resulting proof before it is published in its final form. Please note that during the production process errors may be discovered which could affect the content, and all legal disclaimers that apply to the journal pertain.

Impact of gradient number and voxel size on DTI tractography for resective brain surgery

Friso W.A. Hoefnagels¹, M.D., Philip C. de Witt Hamer¹, M.D., Ph.D., Petra J.W. Pouwels², Ph.D., Frederik Barkhof³, M.D., Ph.D., W. Peter Vandertop¹, M.D., Ph.D.

¹ Neurosurgical Center Amsterdam, VU University medical center;

² Department Physics & Medical Technology, VU University medical center;

³ Department Radiology & Nuclear Medicine, VU University medical center;

Amsterdam, the Netherlands

Corresponding author:

Friso Hoefnagels
Academic Medical Center Amsterdam
Department Neurosurgery

Meibergdreef 9
P.O.Box 226600
1100DD Amsterdam
The Netherlands

Tel. 0031-20-5663316

E-mail: f.w.hoefnagels@amc.nl

Keywords: brain tumor, DTI-tractography, white matter tracts, acquisition parameters, resolution, number of gradients

Abbreviations: CST = corticospinal tract, DTI = diffusion tensor imaging, FA = fractional anisotropy, IFOF = inferior fronto-occipital fasciculus, NGD = number of gradient directions, OR = optic radiation, SLF = superior longitudinal fasciculus, SR = spatial resolution

Abstract

Objective: To explore quantitatively and qualitatively how the number of gradient directions (NGD) and spatial resolution (SR) affect DTI-tractography in patients planned for brain tumor surgery, using routine clinical MR-imaging protocols.

Methods: Of 67 patients with intracerebral lesions who had two different DTI-scans, three DTI-series were reconstructed to compare the effects of NGD and SR. Tractographies for four clinically relevant tracts (corticospinal tract, superior longitudinal fasciculus, optic radiation and inferior fronto-occipital fasciculus) were constructed with a probabilistic tracking algorithm and automated ROI-placement and compared for three quantitative measurements: tract volume, median fiber density and mean FA, using linear mixed-effects models. The mean tractography volume and intersubject reliability were visually compared across scanning protocols, to assess the clinical relevance of the quantitative differences.

Results: Both NGD and SR significantly influenced tract volume, median fiber density and mean FA, but not to the same extent. Especially higher NGD increased tract volume and median fiber density. More importantly, these effects further increased when tracts were affected by pathology. The effects were tract-specific, but not dependent on threshold. The superior longitudinal fasciculus and inferior fronto-occipital fasciculus showed the most significant differences. Qualitative assessment showed larger tract volumes given a fixed confidence level, and better intersubject reliability for the higher NGD-protocol. SR in the range we considered seemed less relevant than NGD.

Conclusion: The current study indicates that, under time constraints of clinical imaging, a higher number of diffusion gradients is more important than spatial resolution for superior DTI probabilistic tractography in patients undergoing brain tumor surgery.

Introduction

Diffusion Tensor Imaging (DTI) is an advanced MRI technique used to study white matter integrity in a variety of diseases, such as Alzheimer, MS or glioma.¹⁻⁴ DTI information is also used to visualize white matter tracts: DTI-tractography.^{5,6} This anatomical reconstruction of well-defined functional subcortical structures supports clinical decision making: it is used for planning a surgical approach in patients with brain tumors and increases the efficiency of intraoperative electrical stimulation, thereby reducing surgical morbidity by avoiding disruption of functional structures.⁷⁻¹¹ Examples of surgically relevant subcortical structures include the corticospinal tract (CST) for motor function, the superior longitudinal fasciculus (SLF) and inferior fronto-occipital fasciculus (IFOF) for language function, and the optic radiation (OR) for vision.¹²⁻¹⁸

Tractography is influenced by many factors, such as tracking algorithm and strategy,¹⁹⁻²⁵ and the quality of the DTI acquisition. DTI is sensitive to noise and influenced by acquisition parameters, such as the number of gradient directions (NGD),²⁶⁻³⁰ spatial resolution,^{29,31} sampling scheme,^{26,27,32,33} number and choice of b-values^{32,34,35} number of scan repetitions,^{28,36,37} field strength³⁸⁻⁴⁰ and scanner hardware.^{20,25,41} Optimization of acquisition parameters can improve tractography, based on phantom studies, simulations or healthy subjects.^{29,34,40,42}

The quantitative measures tract volume, fiber density and (mean) FA are most often used to describe a tractography. Larger tract volumes are often regarded as a positive phenomenon, but do not necessarily indicate superior tractography because of the possibility of false-positive aberrant fibers. Fiber density on the other hand is a measure of tractography robustness. Higher fiber densities correspond with an increased likelihood that a voxel is part of a white matter tract. Aberrant pathways display relatively low fiber densities⁵. The mean FA of the tractography indicates through which regions the fibers were propagated. Tractographies with lower mean FA correspond to fibers in regions of lower certainty, for instance in the periphery of the tract, or at tract-crossings.

Tractographies with high mean FA values tend to display only the core of the white matter tract.

Only few studies have directly explored acquisition effects on tract volume and fiber density, both relevant for surgical decision making,^{23,39,40,43-46} and data on brain tumor patients are lacking. In this setting two challenges must be discerned: (1) the limitation of acquisition time in clinical scanning protocols, resulting in lower signal-to-noise-ratios (SNR) compared to the optimized acquisition protocols used in research, and (2) the presence of tumor-related effects, such as infiltration, disruption and displacement of tracts and brain edema.^{4,47,48} Among the most important factors that influence SNR and reliability are the number of gradient directions and spatial resolution.^{26,29} In this study, we explore the impact of NGD and spatial resolution on quantitative tractography measures in patients with intracerebral lesions involving four surgically relevant fiber tracts using a probabilistic tracking algorithm.

Materials and Methods

Patient selection

A group of 397 patients with newly diagnosed, intra-axial cerebral lesions, whose routine pretreatment clinical MR-scans included DTI-acquisitions, were obtained from our electronic database. Of these, 68 patients were included in whom two different DTI acquisitions had been performed within the same session: one used in the Brainlab neuronavigation system (12 gradient directions protocol), and one used in other protocols for offline evaluation with FSL (FMRIB Software Library) for more complex tractographies (30 gradient directions protocol). The research was performed according to the guidelines and with approval of our institutions Medical Ethics Committee.

Lesion volume and histology were determined for the intra-axial oncological subgroup, consisting of gliomas and metastases, to control for possible confounding effects. A histological diagnosis was obtained from all tumors, and glioma grades were scored according to the WHO-classification. Tumor volumes were estimated in cc's by using the formula: $\text{volume} = \frac{4}{3} * \pi * r_1 * r_2 * r_3$, with r determined as half of the maximal diameter measured in the three orthogonal

radiological planes. Maximal diameters were measured on T1 post-gadolinium MPR scans for gliomas WHO grade 4 and metastases, and on T2 or FLAIR MPR scans for gliomas WHO grade 2 and 3.

MR-Imaging Acquisition

All patients were scanned on 1.5 T MR-scanners (Siemens Medical Solutions, Erlangen, Germany) using an eight-channel or twelve-channel head coil (but within each individual patient the same head coil was used), with uniform diffusion-weighted single shot echo planar imaging protocols. Two imaging protocols were applied: the first protocol (A) consisted of TR/TE 6400/95 ms, 128 x 128 matrix, 40 slices of 3 mm, with 0.6 mm gap, voxel size 2.0 x 2.0 x 3.0 mm, five volumes without directional weighting (b_0) and 30 volumes with non-collinear diffusion gradient directions (b -value 1000 s/mm^2) with an acquisition time of 3min38. The second protocol (B) consisted of TR/TE 10400/90 ms, 128x128 matrix, 67 contiguous 2 mm slices, voxel size 2.0 x 2.0 x 2.0 mm, one volume without directional weighting and 12 volumes with non-collinear diffusion gradient directions (b -value 750 s/mm^2) with an acquisition time of 2min27. All images were visually inspected for absence of motion and ghosting artefacts.

The two available clinical DTI-acquisition protocols differ both in NGD and spatial resolution. To compare the effects of these parameters separately, a subset of 12 diffusion gradient directions was selected from the 30 direction protocol. Since the optimal geometric configuration of the gradient directions is one that is uniformly distributed along the surface of a sphere, to minimize the orientational dependence of the estimated DTI parameters^{26,49}, we optimized a uniformly distributed subset with a total vector summation of <0.001 along each of the orthogonal axes. This third, derived DTI-series (C) thus consisted of 12 gradient directions and a voxel size of 2.0 x 2.0 x 3.0 mm. By comparing series A and C the effect of NGD (12 versus 30) was evaluated, and by comparing series B and C the effect of spatial resolution (2.0 x 2.0 x 2.0 mm versus 2.0 x 2.0 x 3.0 mm voxels) was evaluated.

DTI pre-processing and tractography

DTI-images were processed using FSL 4.0 software (FMRIB Software Library), for each of the three DTI-series. After brain extraction, motion and eddy current correction, the FMRIB's Diffusion Toolbox (FDT) was used for fitting a tensor model to the diffusion data. Next, BEDPOSTX (Bayesian Estimation of Diffusion Parameters Obtained using Sampling Techniques, FSL) was run for all DTI-series to enable probabilistic tractography.

We used a probabilistic tracking algorithm (PROBTRACKX)⁵ with a multiple ROI approach and automated ROI positioning to enhance reproducibility and to reduce intra- and interrater variability, essential for quantitative tractography analysis.^{23,25,50}

To perform automated ROI positioning, first, all subject's Fractional Anisotropy (FA)-maps were registered to FSL's FA-atlas in standard space (FMRIB58_FA), with FNIRT as is customary in TBSS⁵¹, and which is more reliable than affine registration.²⁵ Second, in standard space, the different ROIs for the four white matter tracts were established bilaterally. Third, these ROIs in standard space were warped back to subject space and used for tracking.

Two ROIs were strategically chosen for the corticospinal tract (CST), the superior longitudinal fasciculus (SLF) and the inferior fronto-occipital fasciculus (IFOF), referencing previous fiber tracking methods.^{50,52,53} An exclusion ROI was placed in the contralateral hemisphere to avoid erroneous inclusion of contralateral fibers. To track the optic radiation (OR), one ROI was placed in the lateral geniculate body based on Juelich Histologic Atlas (Zilles and Amunts, provided by Simon Eickhoff, Burgel⁵⁴). A second ROI was placed at the intersection between the atlas-based V1-area and OR. The same contralateral exclusion-ROI as for the other tracts was used, as well as a ROI in the ventral part of the insula covering the IFOF and uncinate fasciculus (UF). Similarity of the automatically positioned ROIs across the different series was confirmed by comparing ROI size and ROI mean FA (data not shown).

Probabilistic tractography was performed by FSL's PROBTRACKX with default parameter settings, except for curvature threshold, which was set to 0 to avoid curvature restrictions, and for FA-constraining. As a last step, thresholds were set to reject implausible fibers. Thresholds were chosen as a percentage of the 98th percentile voxel intensity value. Nine different thresholds were evaluated for each tractography (0.1, 0.2, 0.5, 1, 2, 5, 10, 20 and 50%). Finally, all tracts and ROIs were visually checked and

discarded from further analysis in case of ROI malpositioning. Tractography-failures were scored when no fibers could be displayed.

Finally, all tracts were categorized as "healthy" or "diseased". Tracts were considered healthy when located contralateral to the lesion, or ipsilateral to, remote from and not deviated by the lesions, well outside the T2 hyperintense area. Tracts were otherwise considered "diseased". As a second step, the diseased tracts were further categorized in "mass effect" when outside the T2 hyperintense zone but deviated, and "infiltration/edema" when running through the T2 hyperintense area. Since edema and infiltration cannot be reliably differentiated in glioma patients, this group (edema/infiltration) was not further classified.

Quantitative tractography analysis

Three outcome measures were calculated for each tractography result: the fiber tract volume, the median fiber density and the mean tract FA.

For evaluation of volume, confidence and meanFA of the tractographies we used FSL's probabilistic fibertracking program PROBTRACKX. Tract volume was calculated by multiplying the number of positive voxels included in the tractography by voxel volume. PROBTRACKX returns a map with brain voxels, of which all will have a value (though many of these will be zero) representing the connectivity value between that voxel and the seed voxel (i.e., the number of samples that pass through that voxel). The median connectivity value (or median "fiber density") was used here because it does not follow a normal distribution. FA-values were obtained and averaged for all positive tractography voxels.

Qualitative comparison

The clinical relevance of differences in tractographies due to scanning protocol was qualitatively determined by group display of healthy tractographies for each protocol. This group display enables a direct comparison of (1) differences in intersubject variability of the tractographies (defined as intersubject tractographies), and (2) differences in tract volumes using equal confidence levels (defined as group mean

tractographies). Group level tractographies were reconstructed for the high resolution, low NGD-protocol (series A) and low resolution, high NGD-protocol (series B).

First, all healthy tracts were tracked at the same arbitrary fiber density threshold of 20% and registered to standard space. Next, the two group-tractographies (the intersubject tractography and the group mean tractography) were calculated for each white matter structure. To create intersubject tractographies, the individual tractographies were binarized and stacked in standard space. The intensity of the summated tracts corresponds to the number of patients for which the voxel was included in the tractography. The intersubject tractographies were compared for low (20%) and high (80%) levels of intersubject reliability.

To create group mean tractographies, the tractographies were stacked and averaged. The intensity of each group mean tractography-voxel corresponds to the average fiber density. The group mean tractographies were compared for tract volume when equivalent thresholds were used for both protocols.

Statistical Methods

We used R (RComprehensive R Archive Network, version 3.4.1), *lme4* (Bates, Maechler & Bolker, 2012) and *lmerTest* (Kuznetsova, Brockhoff & Christensen, 2016) to perform a linear mixed effects analysis of the relationship between three tractography outcome measures (volume, median fiber density and mean FA) and acquisition-parameters NGD and resolution .

Tract volume and (median) fiber density show exponential relations (when plotted against threshold). To analyze the data with linear mixed-effects models, the log of volume (log.vol) and median fiber density (log.med.f) were calculated and used for further analysis. Fiber density threshold was plotted against log.vol and log.med.f and loglinearity was confirmed with R-squared ranging between 0.8 and 0.96.

The primary interest consisted of the effect of NGD and resolution (represented by variable "Series") on the tractography measures, under healthy and pathological conditions (represented by variable "Disease-effect"). Series and Disease-effect were entered as fixed effects (without interaction term) into the model. As random effects, we entered intercepts for subjects ("Subject"), fiber density threshold ("Threshold") and subcortical tract ("Tract").

As next steps, we extended the model by sequentially adding 1) an interaction term, between Series and Disease; 2) further specification of Disease effect into “healthy”, “mass effect” and “infiltration/edema”, and 3) adding extra possible confounding covariates “lesion volume” and “histology” (glioma WHO grade 2, 3 or 4 and metastasis) for the oncological subgroup.

Visual inspection of residual plots did not reveal any obvious deviations from normality or homogeneity. P-values were obtained by likelihood ratio tests of the full model with the effect in question against the model without the effect in question.

Results

Clinical characteristics

Visual inspection for artifacts led to the exclusion of one patient (artifacts in all three series). Additionally, for the remaining 67 patients, nine separate series were excluded because of artifacts (Table 1). Of the 67 patients (mean age 48.3 years), 35 were male. The lesions (right-sided in 40) consisted of 42 gliomas (14 WHO grade 2, 13 WHO grade 3 and 15 WHO grade 4), 10 metastases, 8 mesiotemporal sclerosis and 7 other lesions (2 cavernomas, 2 lymphomas, 1 meningioma, 1 venous thrombosis, 1 inconclusive pathology). Patient characteristics, including tumor volume measurements, are presented in Suppl. Table 1.

Visual inspection scans and ROI placement

Registration to standard space was performed successfully for all series. Visual inspection of ROI placement from standard to subject space led to the exclusion of seven ROIs of a total of 2688, and therefore of seven of 1536 (0.46%) tracts (Table 1). According to their relation to the pathology, 1105 tractographies were assigned to the healthy group and 424 in the “diseased” group (Table 1). All but one tractography-failure (no fibers displayed) were in the diseased-group. Series A had 15 failures (10.1% of the “diseased” tracts), series B six failures (4.3%) and series C 16 failures (11.5%). Eighty percent of the failure-cases concerned the IFOF.

Tractographies: quantitative comparisons

A linear mixed effects analysis was performed of the relationship between three tractography outcome measures (volume, median fiber density and mean FA) and scanning-parameters NGD and resolution (reflected by "Series") under healthy and pathological conditions (reflected by "Disease-effect"). Subject, Threshold and Tract were entered as random effects for controlling possible confounding relations. Both "Series" and "Disease-effect" affected all three outcome measures (log.vol, log.median.f, meanFA) significantly, as did all three random effects.

Next, we extended this basic model as described in the Methods section, to find better predictive models (Table 2). First, an interaction effect of Series and Disease was added. A small effect was found for all three outcome measures (log.vol: χ^2 47.5, $p < 0.0001$, log.median.f: χ^2 34.6 $p < 0.0001$, meanFA: χ^2 226.6 $p < 0.0001$). Next, we further improved the model by specification of disease effect by distinguishing "healthy" from "mass effect" from "edema/infiltration". This also affected all three outcome measures (log.vol: χ^2 223.5, $p < 0.0001$, log.median.f: χ^2 118.3 $p < 0.0001$, meanFA: χ^2 158.3 $p < 0.0001$) and improved the model. Finally, the effects of histology and tumor volume were explored for the oncological subgroup (consisting of gliomas and metastases). Expanding the model by covariates histology and tumor volume had no significant effect on neither of the three outcome measures (Table 2).

The effects of this extended superior model (with a further specified Disease-effect and an interaction term for Series and Disease-effect) are presented in Table 3.

Tract volume

The parameters NGD, resolution, mass effect and edema/infiltration all significantly affected tract volume, as demonstrated in Table 3. Higher NGD resulted in larger tract volume, while higher resolution (smaller voxels) and tracts affected by disease (mass effect or edema/infiltration) had smaller tract volumes. NGD and edema/infiltration had relatively large effect sizes (increase of log.vol with 0.45 and decrease of log.vol with -0.66, respectively), compared to the resolution and the mass effect (decrease of -0.16 both). The increase in tract volume with higher NGD was even larger for tracts affected by pathology compared to healthy tracts (log.vol

increase of 0.19), and the decrease of tract volume for higher resolution was largest for tracts suffering from mass effects (log.vol decrease of -0.38) (Table 3). To explore possible differences of NGD and resolution effects on tract volume for different tracts, they were plotted for each tract separately at a single (arbitrary) threshold of 20% (Fig. 1a). Although resolution effects might differ slightly per tract, NGD effects are very consistent across all tracts.

Median fiber density

NGD, resolution, mass effect and edema/infiltration all significantly affected median fiber density (Table 3). Higher NGD and higher resolution increased median fiber density, whereas mass effect and edema/infiltration both decreased median fiber density. The largest effects were demonstrated for NGD and edema/infiltration (change in log.median.f of 1.12 and -1.28, respectively), and smaller effects for resolution and mass effect (0.16 and -0.39, respectively). The effects of high NGD was especially larger for tracts affected by edema/infiltration (increase of log.median.f by 2.43) (Table 3).

To explore possible differences of NGD and resolution effects on fiber density for different tracts, they were plotted for each tract separately at a single (arbitrary) threshold of 20% (Fig. 1b). Although resolution effects might differ slightly per tract, NGD effects are, again, very consistent across all tracts.

Mean tract FA

Again, NGD, resolution, mass effect and edema/infiltration all significantly affected mean FA (Table 3). Edema/infiltration decreased meanFA by -0.07 and NGD by -0.04. The effects of resolution and mass effect were negligible (Table 3).

Tractographies: Qualitative comparison

In Figure 2 the intersubject tractographies of all healthy tracts are displayed in standard space, for the high resolution, low NGD-protocol (series A) and low resolution, high NGD-protocol (series B). As more tractographies of different subjects overlap, the

intersubject tractography increases. Series B showed larger intersubject reliability, as demonstrated by the larger tract volumes, especially for the SLF and the IFOF. This effect of better intersubject reliability is more pronounced, when the intersubject tractographies are displayed at higher concordance levels (positive for 80% of subjects; right side columns of each diagram in Fig. 2). The volumes of the intersubject tractographies are displayed in supplemental Table 2.

Finally, tract volumes were compared when equivalent fiber density thresholds, and therefore the same levels of confidence, were used (group mean tractographies; Fig. 3). The core of the tracts was visualized well for most tracts, using both protocols. However, the high NGD protocol enabled further propagation of the tracts, especially for SLF and IFOF. Tract volumes diminished rapidly when the confidence levels were increased, in case of the low NGD protocol.

Discussion

We explored quantitatively and qualitatively how the number of gradient directions (NGD) and spatial resolution (SR) affect DTI-tractography in patients planned for resective brain surgery. The main findings are that (1) the number of gradient directions has a larger impact on tract volume and fiber density than does spatial resolution, and (2) this differential impact from the number of gradient directions is even larger for tracts involved by pathology than for normal tracts.

In general, a gold standard for tractography has not been defined. Too liberal tracking strategies will overestimate white matter tracts resulting in too limited resections, whereas too strict tracking strategies will underestimate the white matter tracts resulting in increased postoperative neurological deficits. Ideally, DTI-tractography parameter settings could be evaluated and optimized by correlating post-operative functional outcome measures with surgical damage to the pre-operatively defined tractography. For this purpose, the function of the tract should be unambiguous, exclusively attributable to that specific tract, accurately and quantitatively testable, and not susceptible to functional plasticity in case of (surgical) damage. To quantify the amount of damage to the tractography, the pre- and post-operative scans should be

perfectly registered and corrected for three dimensional, post-operative brain shift. The involvement of the tractography should solely be attributable to the resection and not as a consequence of vascular damage or post-operative edema. Given these many requirements, this “gold standard” study remains illusive.

One of the strengths of the current study is the evaluation of complementary quantitative tractography measures by using a probabilistic algorithm instead of deterministic algorithms, which are commonly used in clinical settings. This allows for an estimation of the confidence of the displayed fibers in addition to the conventional tractography volumes, as probabilistic algorithms account for uncertainty of the main direction of the diffusion tensor. Tracking from each voxel is repeated and a probability of connectivity to other regions is generated, based on this uncertainty. The probabilities are expressed as fiber densities and can be interpreted as a relative measure of the confidence assigned to the generated tractography.⁵ This becomes especially evident in case of pathology, when low FA and directional uncertainty are readily encountered.⁴ Instead of discontinuing the fiber propagation as occurs with deterministic algorithms, probabilistic algorithms display multiple options, albeit with lower probability.⁵

In contrast to previous studies using phantoms and healthy subjects, the current study describes the influences of acquisition parameters in patients with tracts involved by brain pathology. Tumor and tumor-related effects such as mass displacement, infiltration and edema, challenge tracking algorithms. We show in concordance with Stadlbauer et al. that pathology reduces not only tract volume, as Bello et al.¹³ also suggested, but, even more importantly, also fiber density.⁵⁵ These negative effects are more pronounced with lower NGD; higher NGD protocols improve tensor estimation and hence tractography results.

The most important limitation of our study is its retrospective nature. The available scan protocols did not have identical scanning times, inducing potential differences in SNR. The short difference in scanning time between our two clinical protocols however, suggests a limited impact on the differences in SNR. Ideally, acquisition parameters other than NGD or resolution would have been identical across the scanning protocols.

For the analysis of NDG-effects, comparisons were made between the 30D protocol and the 30-to-12D protocol. Since this is essentially the same protocol, just after removing 18 gradients directions, all other scan parameters for these protocols are identical, so there are no confounding effects of different acquisition parameters.

For the analysis of resolution effects, the 12NDG protocol and the 30-to-12NDG protocol were compared, and some differences do exist between acquisition parameters, for instance different b-values, and voxel isotropy. B-values affect tensor-shape, and FA-estimation. However, when we consider the level of differences between the b-values used in our protocols (750 and 1000s/mm²), the estimated differences are expected to be very small.³⁵

Voxel anisometry affect tensor shape and tractography. However, in human brains with relatively large fiber tracts, and considering the degree of anisotropy (1:1:1.5), this seems to be of relatively minor importance.⁵⁶

So the amount of uncertainty introduced by these factors is supposed to be small however, compared to NGD and resolution effects.^{26,27,36}

A second limitation of our study is the heterogeneity of our subject group containing multiple pathologies. In terms of relevancy for tractography however, they often bear the same consequences: decreased local FA,^{4,57-59} and hence, increased directional uncertainty.

The demonstrated increase of tract volume with higher NGD, which has been reported previously,^{23,45} is likely the result of better fiber propagation in areas of relative uncertainty of the principal diffusion direction (low FA).^{30,34,35} The reported effects of NGD on fiber density are more contradictory; with the use of higher NGD, the tractographies are expected to be more robust and therefore display higher fiber densities. Some previous studies, all using deterministic tracking algorithms, have reported the expected increase in fiber densities with higher NGD, while others have reported no differences.^{37,44,45} The choice of algorithm might explain the discordance with our results, since fiber densities represent a true relative measure in probabilistic algorithms, whereas binary assumptions underlie the fiber densities in deterministic algorithms. The only study that used the same, probabilistic tracking algorithm as we

did find an increase in tract volume for the higher NGD protocol, in accordance with our results.²³ Unfortunately, the effect of NGD on fiber density was not explored.

All tracts seemed to benefit from higher NGD, but not to the same extent. This tract-specificity is not uncommon for quantitative tractography measurements,^{19,20,29,44,45} and is likely the result of differences in white matter architecture. Tracts with a lower degree of myelination, weaker longitudinal organization or closer proximity to other tracts, with crossing or kissing fiber bundles (e.g. the SLF and IFOF) display lower anisotropy, and therefore suffer more from directional uncertainty. As explained, especially these tracts might benefit more from higher NGD, which reduces this uncertainty. The same superior robustness of the CST and OR have been shown using histological dissection techniques.⁵⁴

The clinical relevance of the quantitative differences we found can probably be best appreciated by visual assessment. Less complex subcortical structures, such as the CST, could be tracked well with all three sequences. This tract showed relatively high fiber densities for all protocols, and the volume differences are predominantly caused by further propagation into grey matter and infratentorially. Higher NGD seems mandatory however, for the reliable tracking of the SLF and IFOF, since it improves robustness, as is reflected in higher fiber density and intersubject reliability, and increases tract volumes in all dimensions along their subcortical courses.

Spatial resolution, in the range we considered, does not seem critical for tracking most structures, and should only be invested in when the requirements of higher NGD are met. Increasing spatial resolution has the theoretical advantage of suffering less from complex intravoxel fiber configurations, such as crossing, kissing, bending and/or splitting fiber bundles,^{35,49,60} but decreases SNR.²⁹ Probabilistic and multitensor tracking algorithms are supposed to handle complex fiber configurations better,^{5,24,61} and possibly suffer less from lower resolution. Our data support this view, since most tractographies showed only minor differences in fiber density or tract volume, when comparing both resolutions.

In neurosurgical practice the optimal tractography would meet the following requirements: (1) estimated confidence levels assigned to the generated tracts, (2) high intersubject reliability, (3) relative insensitivity to changes in threshold settings, and (4) the ability to propagate fibers in areas of relative uncertainty of fiber direction, e.g. in case of pathology. Our data suggest, quantitatively as well as qualitatively, that a higher NGD scanning protocol helps for the last three, and that the number of diffusion gradients is more important than spatial resolution for DTI probabilistic tractography, especially in patients with structural intracerebral lesions.

Conflicts of interest: none

Funding: This research did not receive any specific grant from funding agencies in the public, commercial, or not-for-profit sectors.

Legends

Figure 1. Volumes and fiber densities

In Figure 1A, boxplots show the tract volumes for the different scanning protocols (the red dots indicate the median tract volumes, the boxes outline the 25th to 75th percentiles). Tractographies were constructed with a 20% threshold. The effects for the different tracts (CST, SLF, IFOF and OR) and different conditions (healthy or diseased) are displayed in separate panels. The effect of SR is demonstrated by comparing series A and C, the effect of NGD by comparing series B and C. The NGD effects are larger than the SR effects, especially for the tractographies influenced by disease. The tracts that increase most are CST, SLF and IFOF. Likewise, in Figure 1B the median fiber densities are demonstrated. The same effects are demonstrated for fiber densities as for tract volume.

Figure 2. Intersubject tractographies

Four diagrams are displayed for different tracts: *A.* CST; *B.* IFOF; *C.* OR and *D.* SLF. Each diagram displays the healthy tractographies for the original 12 direction (red – yellow) and 30 direction protocol (dark blue – light blue). The left columns display tract-voxels when positive for at least 20% of the patients. The right column shows tract volumes at a higher concordance level; when positive for 80% of the patients. Brighter colors correspond to a higher number of patients. The effect of higher intersubject reliability is shown for all tracts (larger tract volumes for the 30 direction protocol in all right columns). The effect of larger tract volume at higher NGD is most clearly demonstrated for the IFOF and SLF.

Figure 3. Group mean tractographies

As Figure 2. Mean fiber densities per voxel were calculated by averaging over patients. Equivalent fiber density thresholds were used for the two protocols (low NGD in red – yellow, high NGD in dark – light blue). All tracts (*A.* CST, *B.* IFOF, *C.* OR and *D.* SLF)

show larger volumes with higher mean fiber densities for the higher NGD protocol, but most clearly for IFOF and SLF.

ACCEPTED MANUSCRIPT

References

1. Damoiseaux JS, Smith SM, Witter MP, et al. White matter tract integrity in aging and Alzheimer's disease. *Hum Brain Mapp* 2009; **30**(4): 1051-9.
2. Kern KC, Sarcona J, Montag M, Giesser BS, Sicotte NL. Corpus callosal diffusivity predicts motor impairment in relapsing-remitting multiple sclerosis: A TBSS and tractography study. *Neuroimage* 2011; **55**(3): 1169-77.
3. Roosendaal SD, Geurts JJ, Vrenken H, et al. Regional DTI differences in multiple sclerosis patients. *Neuroimage* 2009; **44**(4): 1397-403.
4. Stadlbauer A, Ganslandt O, Buslei R, et al. Gliomas: histopathologic evaluation of changes in directionality and magnitude of water diffusion at diffusion-tensor MR imaging. *Radiology* 2006; **240**(3): 803-10.
5. Behrens TE, Berg HJ, Jbabdi S, Rushworth MF, Woolrich MW. Probabilistic diffusion tractography with multiple fibre orientations: What can we gain? *Neuroimage* 2007; **34**(1): 144-55.
6. Mori S, van Zijl PC. Fiber tracking: principles and strategies - a technical review. *NMR Biomed* 2002; **15**(7-8): 468-80.
7. Castellano A, Bello L, Michelozzi C, et al. Role of diffusion tensor magnetic resonance tractography in predicting the extent of resection in glioma surgery. *Neuro Oncol* 2012; **14**(2): 192-202.
8. Kuhnt D, Bauer MH, Becker A, et al. Intraoperative visualization of fiber tracking based reconstruction of language pathways in glioma surgery. *Neurosurgery* 2012; **70**(4): 911-9.
9. Nimsky C, Ganslandt O, Hastreiter P, et al. Preoperative and intraoperative diffusion tensor imaging-based fiber tracking in glioma surgery. *Neurosurgery* 2005; **56**(1): 130-7.
10. Romano A, D'Andrea G, Minniti G, et al. Pre-surgical planning and MR-tractography utility in brain tumour resection. *Eur Radiol* 2009; **19**(12): 2798-808.
11. Zhu FP, Wu JS, Song YY, et al. Clinical application of motor pathway mapping using diffusion tensor imaging tractography and intraoperative direct subcortical stimulation in cerebral glioma surgery: a prospective cohort study. *Neurosurgery* 2012; **71**(6): 1170-83.
12. Bello L, Gallucci M, Fava M, et al. Intraoperative subcortical language tract mapping guides surgical removal of gliomas involving speech areas. *Neurosurgery* 2007; **60**(1): 67-80.
13. Bello L, Gambini A, Castellano A, et al. Motor and language DTI Fiber Tracking combined with intraoperative subcortical mapping for surgical removal of gliomas. *Neuroimage* 2008; **39**(1): 369-82.
14. Duffau H, Peggy Gatignol ST, Mandonnet E, Capelle L, Taillandier L. Intraoperative subcortical stimulation mapping of language pathways in a consecutive series of 115 patients with Grade II glioma in the left dominant hemisphere. *J Neurosurg* 2008; **109**(3): 461-71.
15. Kamada K, Todo T, Masutani Y, et al. Combined use of tractography-integrated functional neuronavigation and direct fiber stimulation. *J Neurosurg* 2005; **102**(4): 664-72.
16. Kamada K, Todo T, Morita A, et al. Functional monitoring for visual pathway using real-time visual evoked potentials and optic-radiation tractography. *Neurosurgery* 2005; **57**(1 Suppl): 121-7.

17. Leclercq D, Duffau H, Delmaire C, et al. Comparison of diffusion tensor imaging tractography of language tracts and intraoperative subcortical stimulations. *J Neurosurg* 2009.
18. Okada T, Mikuni N, Miki Y, et al. Corticospinal tract localization: integration of diffusion-tensor tractography at 3-T MR imaging with intraoperative white matter stimulation mapping--preliminary results. *Radiology* 2006; **240**(3): 849-57.
19. Ciccarelli O, Parker GJ, Toosy AT, et al. From diffusion tractography to quantitative white matter tract measures: a reproducibility study. *Neuroimage* 2003; **18**(2): 348-59.
20. Danielian LE, Iwata NK, Thomasson DM, Floeter MK. Reliability of fiber tracking measurements in diffusion tensor imaging for longitudinal study. *Neuroimage* 2010; **49**(2): 1572-80.
21. Feigl GC, Hiergeist W, Fellner C, et al. MRI diffusion tensor tractography: Evaluation of anatomical accuracy of different fiber tracking software packages. *World Neurosurg* 2013.
22. Fillard P, Descoteaux M, Goh A, et al. Quantitative evaluation of 10 tractography algorithms on a realistic diffusion MR phantom. *Neuroimage* 2011; **56**(1): 220-34.
23. Heiervang E, Behrens TE, Mackay CE, Robson MD, Johansen-Berg H. Between session reproducibility and between subject variability of diffusion MR and tractography measures. *Neuroimage* 2006; **33**(3): 867-77.
24. Tensaouti F, Lahlou I, Clarisse P, Lotterie JA, Berry I. Quantitative and reproducibility study of four tractography algorithms used in clinical routine. *J Magn Reson Imaging* 2011; **34**(1): 165-72.
25. Vollmar C, O'Muircheartaigh J, Barker GJ, et al. Identical, but not the same: intra-site and inter-site reproducibility of fractional anisotropy measures on two 3.0T scanners. *Neuroimage* 2010; **51**(4): 1384-94.
26. Jones DK. The effect of gradient sampling schemes on measures derived from diffusion tensor MRI: a Monte Carlo study. *Magn Reson Med* 2004; **51**(4): 807-15.
27. Landman BA, Farrell JA, Jones CK, Smith SA, Prince JL, Mori S. Effects of diffusion weighting schemes on the reproducibility of DTI-derived fractional anisotropy, mean diffusivity, and principal eigenvector measurements at 1.5T. *Neuroimage* 2007; **36**(4): 1123-38.
28. Ni H, Kavcic V, Zhu T, Ekholm S, Zhong J. Effects of number of diffusion gradient directions on derived diffusion tensor imaging indices in human brain. *AJNR Am J Neuroradiol* 2006; **27**(8): 1776-81.
29. Zhan L, Jahanshad N, Ennis DB, et al. Angular versus spatial resolution trade-offs for diffusion imaging under time constraints. *Hum Brain Mapp* 2012.
30. Zhan L, Leow AD, Jahanshad N, et al. How does angular resolution affect diffusion imaging measures? *Neuroimage* 2010; **49**(2): 1357-71.
31. Oouchi H, Yamada K, Sakai K, et al. Diffusion anisotropy measurement of brain white matter is affected by voxel size: underestimation occurs in areas with crossing fibers. *AJNR Am J Neuroradiol* 2007; **28**(6): 1102-6.
32. Gao W, Zhu H, Lin W. A unified optimization approach for diffusion tensor imaging technique. *Neuroimage* 2009; **44**(3): 729-41.
33. Hasan KM, Parker DL, Alexander AL. Comparison of gradient encoding schemes for diffusion-tensor MRI. *J Magn Reson Imaging* 2001; **13**(5): 769-80.
34. Correia MM, Carpenter TA, Williams GB. Looking for the optimal DTI acquisition scheme given a maximum scan time: are more b-values a waste of time? *Magn Reson Imaging* 2009; **27**(2): 163-75.

35. Jones DK, Basser PJ. "Squashing peanuts and smashing pumpkins": how noise distorts diffusion-weighted MR data. *Magn Reson Med* 2004; **52**(5): 979-93.
36. Farrell JA, Landman BA, Jones CK, et al. Effects of signal-to-noise ratio on the accuracy and reproducibility of diffusion tensor imaging-derived fractional anisotropy, mean diffusivity, and principal eigenvector measurements at 1.5 T. *J Magn Reson Imaging* 2007; **26**(3): 756-67.
37. Widjaja E, Mahmoodabadi SZ, Rea D, Moineddin R, Vidarsson L, Nilsson D. Effects of gradient encoding and number of signal averages on fractional anisotropy and fiber density index in vivo at 1.5 tesla. *Acta Radiol* 2009; **50**(1): 106-13.
38. Huisman TA, Loenneker T, Barta G, et al. Quantitative diffusion tensor MR imaging of the brain: field strength related variance of apparent diffusion coefficient (ADC) and fractional anisotropy (FA) scalars. *Eur Radiol* 2006.
39. Okada T, Miki Y, Fushimi Y, et al. Diffusion-tensor fiber tractography: intraindividual comparison of 3.0-T and 1.5-T MR imaging. *Radiology* 2006; **238**(2): 668-78.
40. Polders DL, Leemans A, Hendrikse J, Donahue MJ, Luijten PR, Hoogduin JM. Signal to noise ratio and uncertainty in diffusion tensor imaging at 1.5, 3.0, and 7.0 Tesla. *J Magn Reson Imaging* 2011; **33**(6): 1456-63.
41. Takao H, Hayashi N, Kabasawa H, Ohtomo K. Effect of scanner in longitudinal diffusion tensor imaging studies. *Hum Brain Mapp* 2011.
42. Jones DK. Determining and visualizing uncertainty in estimates of fiber orientation from diffusion tensor MRI. *Magn Reson Med* 2003; **49**(1): 7-12.
43. Kim M, Ronen I, Ugurbil K, Kim DS. Spatial resolution dependence of DTI tractography in human occipito-callosal region. *Neuroimage* 2006; **32**(3): 1243-9.
44. Lebel C, Benner T, Beaulieu C. Six is enough? Comparison of diffusion parameters measured using six or more diffusion-encoding gradient directions with deterministic tractography. *Magn Reson Med* 2012; **68**(2): 474-83.
45. Wang JY, Abdi H, Bakhadirov K, az-Arrastia R, Devous MD, Sr. A comprehensive reliability assessment of quantitative diffusion tensor tractography. *Neuroimage* 2012; **60**(2): 1127-38.
46. Yamamoto A, Miki Y, Urayama S, et al. Diffusion tensor fiber tractography of the optic radiation: analysis with 6-, 12-, 40-, and 81-directional motion-probing gradients, a preliminary study. *AJNR Am J Neuroradiol* 2007; **28**(1): 92-6.
47. Mori S, Frederiksen K, van Zijl PC, et al. Brain white matter anatomy of tumor patients evaluated with diffusion tensor imaging. *Ann Neurol* 2002; **51**(3): 377-80.
48. Witwer BP, Moftakhar R, Hasan KM, et al. Diffusion-tensor imaging of white matter tracts in patients with cerebral neoplasm. *J Neurosurg* 2002; **97**(3): 568-75.
49. Mukherjee P, Berman JI, Chung SW, Hess CP, Henry RG. Diffusion tensor MR imaging and fiber tractography: theoretic underpinnings. *AJNR Am J Neuroradiol* 2008; **29**(4): 632-41.
50. Huang H, Zhang J, van Zijl PC, Mori S. Analysis of noise effects on DTI-based tractography using the brute-force and multi-ROI approach. *Magn Reson Med* 2004; **52**(3): 559-65.
51. Smith SM, Jenkinson M, Johansen-Berg H, et al. Tract-based spatial statistics: voxelwise analysis of multi-subject diffusion data. *Neuroimage* 2006; **31**(4): 1487-505.
52. Catani M, Thiebaut de SM. A diffusion tensor imaging tractography atlas for virtual in vivo dissections. *Cortex* 2008; **44**(8): 1105-32.
53. Wakana S, Jiang H, Nagae-Poetscher LM, van Zijl PC, Mori S. Fiber tract-based atlas of human white matter anatomy. *Radiology* 2004; **230**(1): 77-87.

54. Burgel U, Amunts K, Hoemke L, Mohlberg H, Gilsbach JM, Zilles K. White matter fiber tracts of the human brain: three-dimensional mapping at microscopic resolution, topography and intersubject variability. *Neuroimage* 2006; **29**(4): 1092-105.
55. Stadlbauer A, Nimsy C, Gruber S, et al. Changes in fiber integrity, diffusivity, and metabolism of the pyramidal tract adjacent to gliomas: a quantitative diffusion tensor fiber tracking and MR spectroscopic imaging study. *AJNR Am J Neuroradiol* 2007; **28**(3): 462-9.
56. Tudela R, Munoz-Moreno E, Lopez-Gil X, Soria G. Effects of Orientation and Anisometry of Magnetic Resonance Imaging Acquisitions on Diffusion Tensor Imaging and Structural Connectomes. *PLoS One* 2017; **12**(1): e0170703.
57. Kinoshita M, Goto T, Okita Y, et al. Diffusion tensor-based tumor infiltration index cannot discriminate vasogenic edema from tumor-infiltrated edema. *J Neurooncol* 2010; **96**(3): 409-15.
58. Lu S, Ahn D, Johnson G, Cha S. Peritumoral diffusion tensor imaging of high-grade gliomas and metastatic brain tumors. *AJNR Am J Neuroradiol* 2003; **24**(5): 937-41.
59. Provenzale JM, McGraw P, Mhatre P, Guo AC, Delong D. Peritumoral brain regions in gliomas and meningiomas: investigation with isotropic diffusion-weighted MR imaging and diffusion-tensor MR imaging. *Radiology* 2004; **232**(2): 451-60.
60. Lazar M, Alexander AL. An error analysis of white matter tractography methods: synthetic diffusion tensor field simulations. *Neuroimage* 2003; **20**(2): 1140-53.
61. Chung HW, Chou MC, Chen CY. Principles and limitations of computational algorithms in clinical diffusion tensor MR tractography. *AJNR Am J Neuroradiol* 2011; **32**(1): 3-13.

Table 1. Registration, ROI placement and Tracts for analysis

		12 DIR		30 DIR		30 to 12 DIR	
Patients		68		68		68	
Scan artifacts		3		4		5	
Scans for ROI placement		65		64		63	
ROI misplacement							
	CST	0/260		0/256		1/252 malposition	
	SLF	1/260 suboptimal		2/256 malposition		0/252	
	OR	0/130		0/128		0/126	
	IFOF	1/260 suboptimal 2/260 malposition		0/256		0/252	
Total discarded ROIs		4/910		2/896		1/882	
Tracts for analysis							
Subgroup		H	D	H	D	H	D
	CST	89	41	88	40	86	39
	SLF	84	45	82	44	83	43
	OR	103	27	101	27	99	27
	IFOF	96	31	98	30	96	30

Tractographies available for analysis according to series (12 DIR, 30 DIR or 30to12 DIR), subcortical structure (CST= cortico-spinal tract, SLF = superior longitudinal fasciculus, OR = optic radiation, IFOF = inferior fronto-occipital fasciculus) and condition (H = healthy, D =diseased). The number of discarded ROIs and tractographies as a consequence of malposition is limited (0.26%).

Table 2. Model comparisons

Parameter	Effect	Data	Model	AIC	LogLik	χ^2	χ df	p
Log.vol	Interaction Series and Disease	Complete set	No interaction	21055	-10519	47.5	2	<0.0001
			Interaction	21011	-10496			
	Specification Disease effect	Complete set	Not specified	21011	-10496	224	3	<0.0001
			Specified	20794	-10384			
	Histology as covariate	Oncological subgroup	- histology	17054	-8513.7	4.7	3	0.1977
			+ histology	17055	-8511.4			
	Tumor volume as covariate	Oncological subgroup	- tumor volume	17054	-8513.7	1.3	1	0.2606
			+ tumor volume	17054	-8413.1			
		Onc. subgroup, affected tracts	- tumor volume	6982	7043.2	0.86	1	0.3528
			+ tumor volume	6983	7050.4			
Log.med.f	Interaction Series and Disease	Complete set	No interaction	46623	-23304	34.6	2	<0.0001
			Interaction	46592	-23286			
	Specification Disease effect	Complete set	Not specified	46592	-23286	118	3	<0.0001
			Specified	46480	-23227			
	Histology as covariate	Oncological subgroup	- histology	36851	-18412	3.2	3	0.3635
			+ histology	35854	-48411			
	Tumor volume as covariate	Oncological subgroup	- tumor volume	36851	-18412	0	1	1
			+ tumor volume	36853	-18412			
		Onc. subgroup, affected tracts	- tumor volume	12696	-6338.2	0	1	1
			+ tumor volume	12698	-6338.2			
MeanFA	Interaction Series and Disease	Complete set	No interaction	-37634	18825	227	2	<0.0001
			Interaction	-37857	18938			
	Specification Disease effect	Complete set	Not specified	-37857	18938	158	3	<0.0001
			Specified	-38009	19018			
	Histology as covariate	Oncological subgroup	- histology	-28959	14493	2.26	3	0.5195
			+ histology	-28955	14494			
	Tumor volume as covariate	Oncological subgroup	- tumor volume	-28959	14493	0	1	1
			+ tumor volume	-28957	14493			
		Onc. subgroup, affected tracts	- tumor volume	-6250	3134.9	0	1	1
			+ tumor volume	-6248	3134.9			

In Table 2 the effects of extending the basic model (with fixed effects: Series and Disease (not further specified) and without interaction component, and random effects: Threshold, Subject and Tract) are presented. The column "parameter" describes the specific outcome measure, the column

“effect” describes the added component/variable to the basic model. AIC = Akaike’s Information Criterion (smaller values indicate superior models), log.Lik = logLikelihood, χ^2 relates to the difference of the two models compared, df = (Satterthwaite approximation of) degrees of freedom, and p = p-value (with Satterthwaite approximation for degrees of freedom). P-values <0.05 are considered significant.

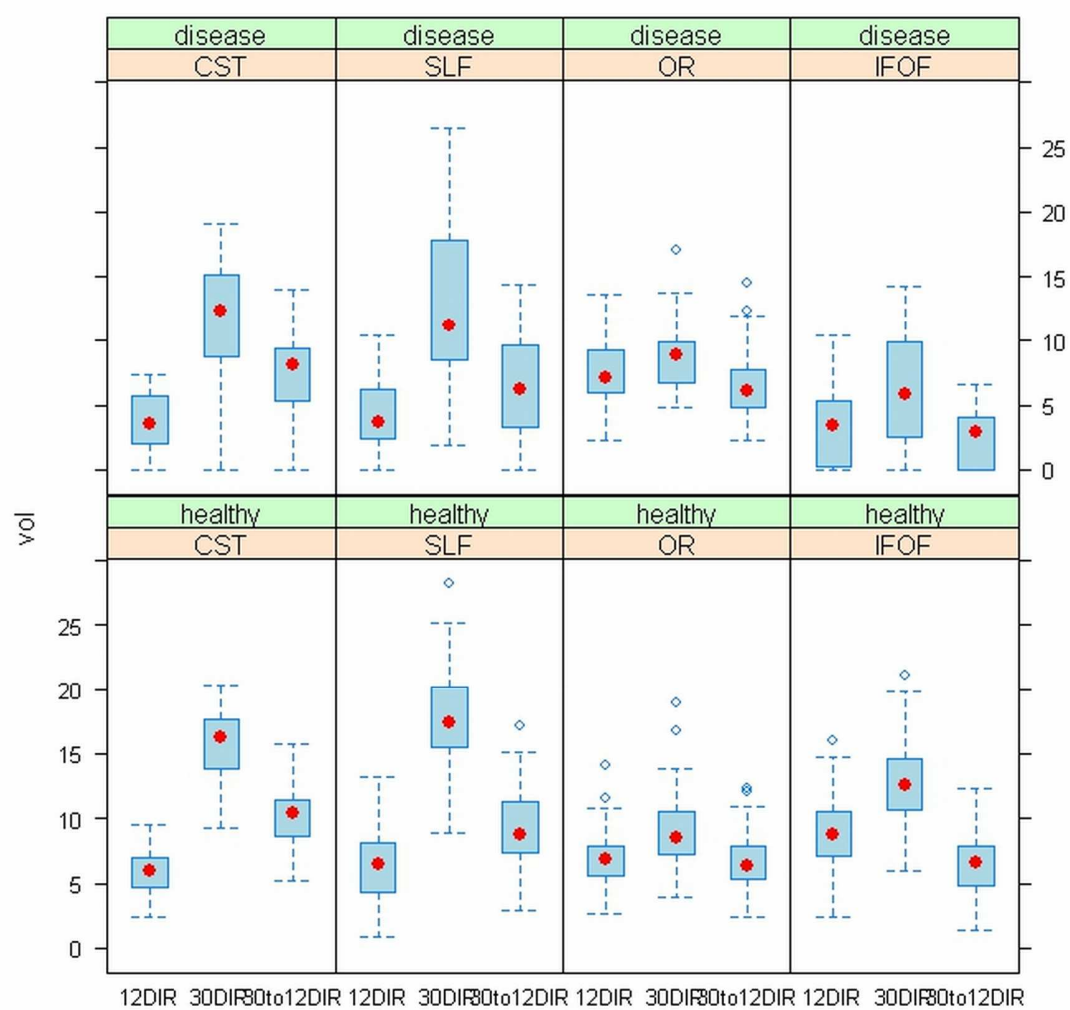
ACCEPTED MANUSCRIPT

Table 3. Results of Linear Mixed Effect Regression Models

Outcome measure: log.vol					
ANOVA Fixed effects	F-value	P	Random effects	χ^2	P
Series	969.0	<0.0001	Threshold	16735	<0.0001
Disease Effect (specified)	1273.3	<0.0001	Subject	1664	<0.0001
Series*Disease Effect	35.5	<0.0001	Tract	934	<0.0001
Fixed Effects	Estimate	SE	t-value	P	
Intercept	2.770	0.2890	9.586	<0.0001	
NGD	0.4536	0.0125	36.306	<0.0001	
Resolution	-0.1557	0.0125	-12.442	<0.0001	
Mass effect	-0.1640	0.0344	-4.767	<0.0001	
Edema/infiltration	-0.6673	0.0188	-35.434	<0.0001	
NGD*Mass effect	-0.0429	0.0469	-0.916	0.36	
NGD*Edema/infiltration	0.1963	0.0258	7.610	<0.0001	
Resolution*Mass effect	-0.3802	0.0469	-8.110	<0.0001	
Resolution*Edema/Infilt.	0.1085	0.0258	4.223	<0.0001	
Outcome measure: log.median.f					
ANOVA Fixed effects	F-value	P	Random effects	χ^2	P
Series	438.4	<0.0001	Threshold	11569	<0.0001
Disease Effect (specified)	928.7	<0.0001	Subject	1052	<0.0001
Series*Disease Effect	13.2	<0.0001	Tract	1739	<0.0001
Fixed Effects	Estimate	SE	t-value	P	
Intercept	5.164	0.5938	8.695	<0.0001	
NGD	1.120	0.0317	35.367	<0.0001	
Resolution	0.161	0.0317	5.073	<0.0001	
Mass effect	-0.393	0.0872	-4.505	<0.0001	

Edema/infiltration	-1.277	0.0477	-26.762	<0.0001
NGD*Mass effect	-0.156	0.1188	-1.309	0.1905
NGD*Edema/infiltration	2.426	0.0654	3.711	0.0002
Resolution*Mass effect	-0.610	0.1189	-5.128	<0.0001
Resolution*Edema/Infiltr.	-0.084	0.0651	-1.283	0.1995
Outcome measure: meanFA				
ANOVA Fixed effects	F-value	P	Random effects	χ^2 P
Series	239.2	<0.0001	Threshold	4742 <0.0001
Disease Effect (specified)	642.3	<0.0001	Subject	1529 <0.0001
Series*Disease (Effect)	72.2	<0.0001	Tract	3151 <0.0001
Fixed Effects	Estimate	SE	t-value	P
Intercept	0.3935	0.02299	17.118	<0.0001
NGD	-0.0437	0.0015	-29.308	<0.0001
Resolution	0.0061	0.0015	4.077	<0.0001
Mass effect	-0.0254	0.0041	-6.188	<0.0001
Edema/infiltration	-0.0771	0.0022	-34.327	<0.0001
NGD*Mass effect	0.0059	0.0056	1.062	0.288
NGD*Edema/infiltration	0.0051	0.0031	16.521	<0.0001
Resolution*Mass effect	0.0078	0.0056	1.395	0.163
Resolution*Edema/Infiltr.	0.0036	0.0031	11.654	<0.0001

In Table 3 the results of the best predictive models are summarized for all three outcome measures. This models constitute Series, Disease Effect (further specified in “healthy”, “mass effect” and “edema/infiltration”) and the interaction between Series*Disease Effect (specified) as Fixed Effects, and Threshold, Subject and Tract as Random Effects. First, the relevance of each of the specific Fixed Effect variables are presented by F- and p-values. Next, the relevance of each of the specific Random Effect variables are presented by χ^2 and p-values. Finally, the Estimates and Standard Errors (SE) are separately reported for each level of the Fixed Effects, to demonstrate the amount of change of the outcome measure and the direction (positive = increase, negative = decrease), and the t- and p-values for the significance of this effect.



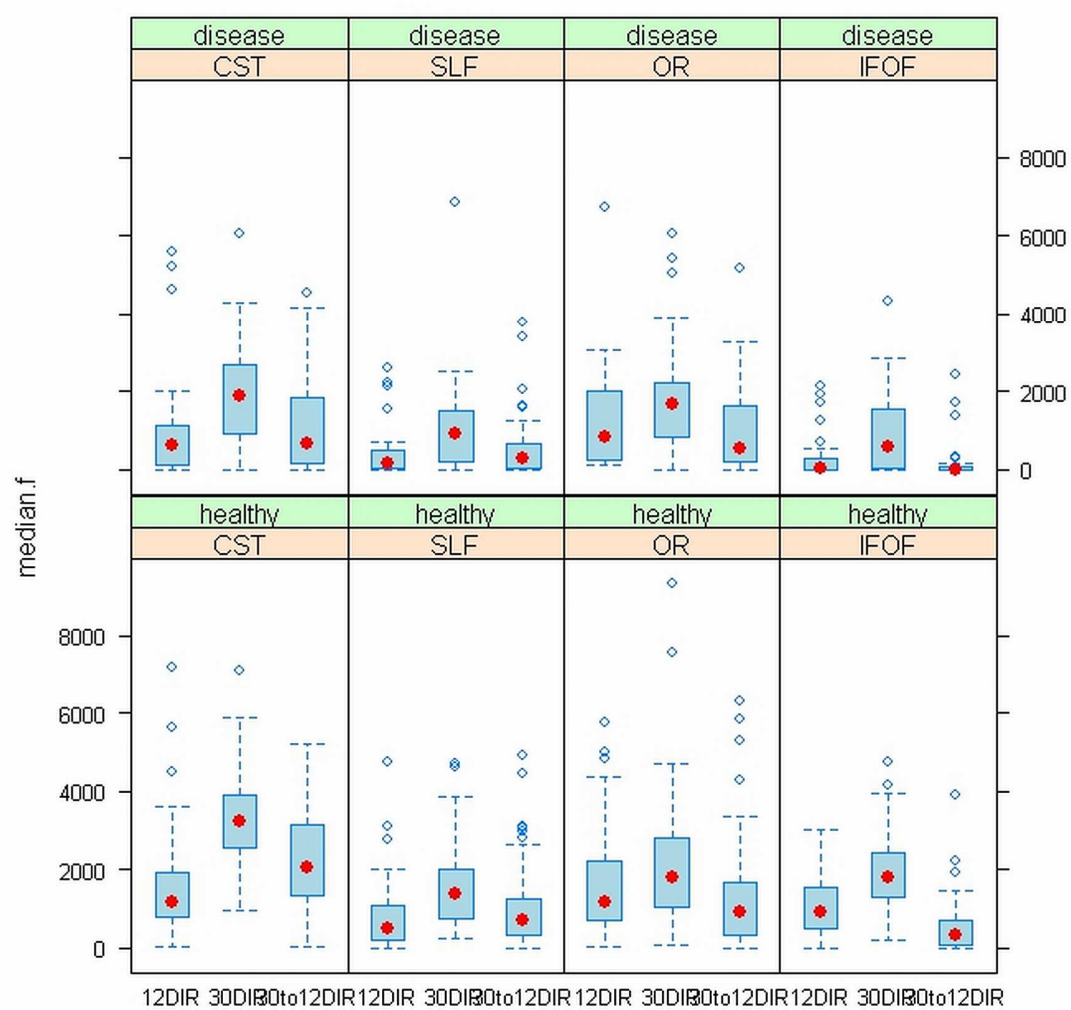


Figure 2

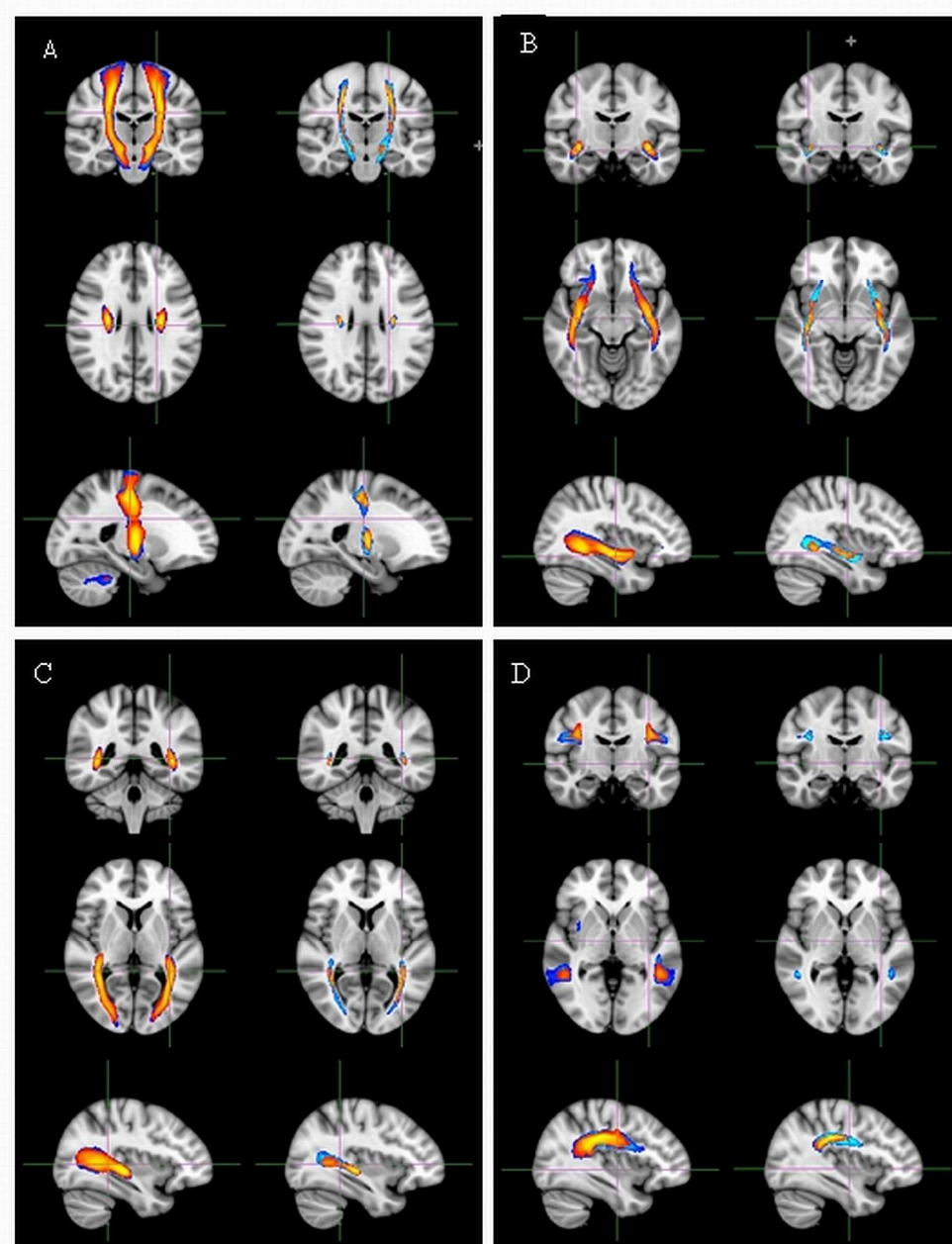
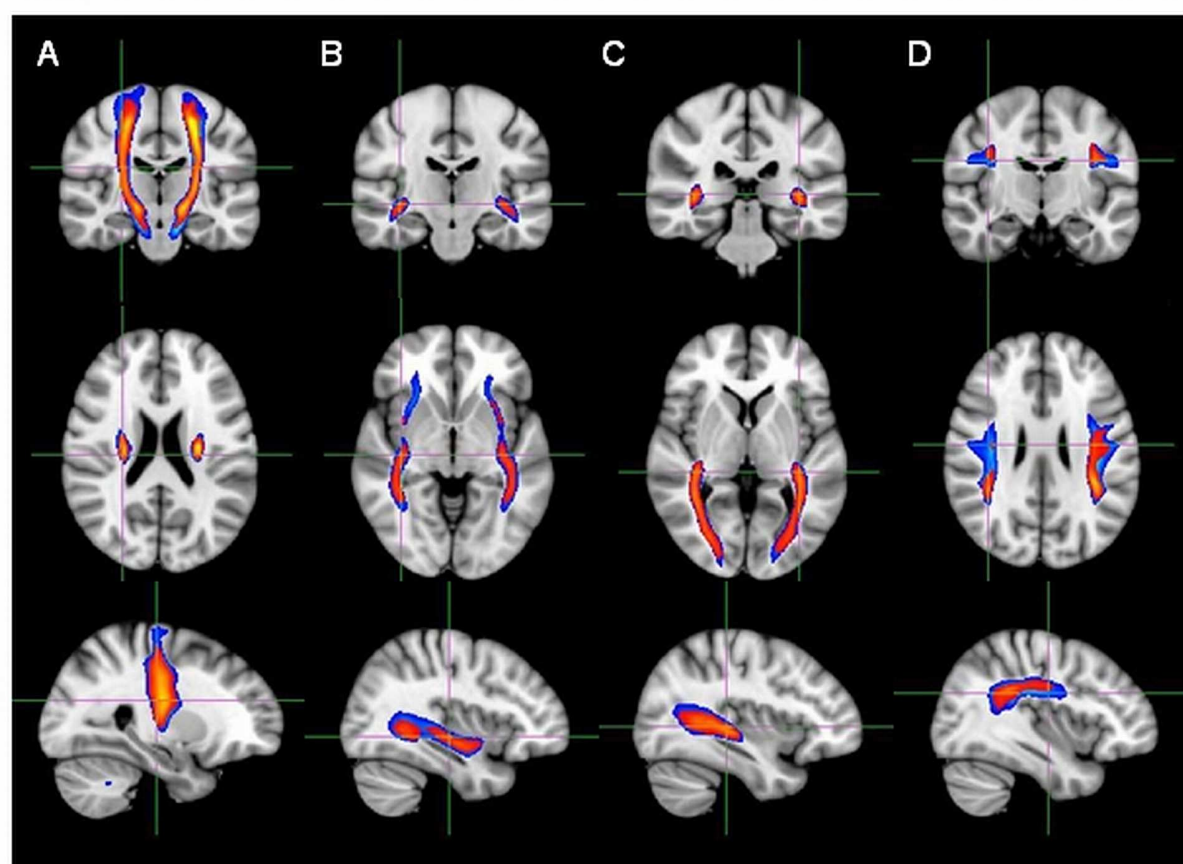


Figure 3



ACCEPTED

Highlights:

- The number of gradient directions (NGD) has a large impact on tract volume and fiber density, larger than for spatial resolution
- The impact from NGD is even larger for tracts involved by pathology than for normal tracts, which is especially important in clinical practice of tumor surgery
- The magnitude of these effects of NGD and resolution is dependent on the specific tract
- For a reliable tracking of more complex fasciculi (e.g. superior longitudinal fasciculus and inferior fronto-occipital fasciculus) higher NGD seems mandatory

Suppl. Table 1. Patient characteristics

Subject	Sex	Age (Years)	Histology	Tumor Volume (cc)
1	M	48	glioma WHO 2	22,2
2	F	55	glioma WHO 2	1,0
3	M	40	glioma WHO 2	71,7
4	M	41	glioma WHO 2	47,3
5	F	39	glioma WHO 2	106,2
6	F	56	glioma WHO 2	149,2
7	M	42	glioma WHO 2	28,4
8	M	31	glioma WHO 2	66,8
9	M	34	glioma WHO 2	17,3
10	M	60	glioma WHO 2	211,9
11	F	39	glioma WHO 2	86,7
12	F	57	glioma WHO 2	112,1
13	F	50	glioma WHO 2	41,3
14	F	31	glioma WHO 2	1,9
15	M	67	glioma WHO 3	128,6
16	F	55	glioma WHO 3	206,2
17	M	52	glioma WHO 3	86,4
18	M	48	glioma WHO 3	101,2
19	M	45	glioma WHO 3	89,6
20	M	62	glioma WHO 3	233,2
21	M	71	glioma WHO 3	216,7
22	F	49	glioma WHO 3	125,1
23	F	63	glioma WHO 3	41,2
24	M	48	glioma WHO 3	8,6
25	M	61	glioma WHO 3	101,6
26	F	45	glioma WHO 3	133,8
27	F	50	glioma WHO 3	32,3
28	M	26	glioma WHO 4	108,4
29	M	56	glioma WHO 4	61,2
30	M	57	glioma WHO 4	68,0
31	F	63	glioma WHO 4	13,4
32	M	65	glioma WHO 4	92,1
33	M	68	glioma WHO 4	143,9
34	M	64	glioma WHO 4	63,8
35	F	59	glioma WHO 4	13,2
36	M	46	glioma WHO 4	74,5
37	F	39	glioma WHO 4	65,5
38	F	67	glioma WHO 4	24,6
39	M	56	glioma WHO 4	3,4
40	M	64	glioma WHO 4	16,3
41	M	58	glioma WHO 4	31,1
42	F	63	glioma WHO 4	44,3
43	M	59	metastasis	2,6
44	M	51	metastasis	70,7
45	F	58	metastasis	6,1
46	M	42	metastasis	34,6

47	M	57	metastasis	10,7
48	M	29	metastasis	1,2
49	M	68	metastasis	19,9
50	F	52	metastasis	6,9
51	M	70	metastasis	0,4
52	F	64	metastasis	6,8
53	F	22	MTS	-
54	M	29	MTS	-
55	F	43	MTS	-
56	F	25	MTS	-
57	M	46	MTS	-
58	M	28	MTS	-
59	F	34	MTS	-
60	F	36	MTS	-
61	F	50	meningeoma	-
62	F	71	lymphoma	-
63	F	44	meningeoma	-
64	F	31	thromboflebitis	-
65	F	42	cavernoma	-
66	F	27	cavernoma	-
67	F	37	glioma, no PA	-

Supplemental Table 1. Intersubject reliability

Tract	Volume (cc)			
	20% intersubject agreement		80% intersubject agreement	
	Series A	Series B	Series A	Series B
CST left	14.0	23.0	3.2	6.6
CST right	14.7	23.2	2.6	6.8
IFOF left	14.7	21.8	2.4	7.0
IFOF right	12.9	19.8	2.3	6.2
OR left	10.9	13.1	1.7	3.8
OR right	11.1	13.1	1.5	3.7
SLF left	12.3	22.7	1.7	6.1
SLF right	10.1	23.7	1.1	5.9

Volumes of the tracts depicted in Figure 2. Series A = 12 directions protocol, series B = 30 directions protocol.

Abbreviations: CST = corticospinal tract, DTI = diffusion tensor imaging, FA = fractional anisotropy, IFOF = inferior fronto-occipital fasciculus, NGD = number of gradient directions, OR = optic radiation, SLF = superior longitudinal fasciculus, SR = spatial resolution

ACCEPTED MANUSCRIPT

AUTHOR DECLARATION

We wish to confirm that there are no known conflicts of interest associated with this publication and there has been no significant financial support for this work that could have influenced its outcome.

We confirm that the manuscript has been read and approved by all named authors and that there are no other persons who satisfied the criteria for authorship but are not listed. We further confirm that the order of authors listed in the manuscript has been approved by all of us.

We confirm that we have given due consideration to the protection of intellectual property associated with this work and that there are no impediments to publication, including the timing of publication, with respect to intellectual property. In so doing we confirm that we have followed the regulations of our institutions concerning intellectual property.

We further confirm that any aspect of the work covered in this manuscript that has involved either experimental animals or human patients has been conducted with the ethical approval of all relevant bodies and that such approvals are acknowledged within the manuscript.

We understand that the Corresponding Author is the sole contact for the Editorial process (including Editorial Manager and direct communications with the office). He is responsible for communicating with the other authors about progress, submissions of revisions and final approval of proofs. We confirm that we have provided a current, correct email address which is accessible by the Corresponding Author and which has been configured to accept email from f.w.hoefnagels@amc.nl

Friso Hoefnagels